



HAL
open science

Humic-like acids from hydrochars: Study of the metal complexation properties compared with humic acids from anthropogenic soils using PARAFAC and time-resolved fluorescence

João Vitor Do Santos, Lais Gomes Fregolente, Altair Benedito Moreira, Odair Pastor Ferreira, Stéphane Mounier, Bruno Viguier, Houssam Hajjoul, Márcia Cristina Bisinoti

► To cite this version:

João Vitor Do Santos, Lais Gomes Fregolente, Altair Benedito Moreira, Odair Pastor Ferreira, Stéphane Mounier, et al.. Humic-like acids from hydrochars: Study of the metal complexation properties compared with humic acids from anthropogenic soils using PARAFAC and time-resolved fluorescence. *Science of the Total Environment*, In press, 10.1016/j.scitotenv.2020.137815 . hal-02507306

HAL Id: hal-02507306

<https://hal.science/hal-02507306v1>

Submitted on 26 May 2020

HAL is a multi-disciplinary open access archive for the deposit and dissemination of scientific research documents, whether they are published or not. The documents may come from teaching and research institutions in France or abroad, or from public or private research centers.

L'archive ouverte pluridisciplinaire **HAL**, est destinée au dépôt et à la diffusion de documents scientifiques de niveau recherche, publiés ou non, émanant des établissements d'enseignement et de recherche français ou étrangers, des laboratoires publics ou privés.

1
2
3
4
5
6
7
8
9
10
11
12
13
14
15
16
17
18
19
20
21
22
23
24
25
26
27
28
29
30
31
32
33
34
35
36
37
38
39
40
41
42
43
44
45
46
47
48
49
50
51
52
53
54
55
56
57
58
59
60
61
62
63
64
65

Humic-like acids from hydrochars: Study of the metal complexation properties compared with humic acids from anthropogenic soils using PARAFAC and time-resolved fluorescence

João Vitor do Santos^a, Lais Gomes Fregolente^{a,b}, Altair Benedito Moreira^a, Odair Pastor Ferreira^b, Stéphane Mounier^c, Bruno Viguiet^c, Houssam Hajjoul^c, and Márcia Cristina Bisinoti^{a*}

^a Laboratório de Estudos em Ciências Ambientais, Departamento de Química e Ciências Ambientais, Instituto de Biociências, Letras e Ciências Exatas, Universidade Estadual Paulista “Júlio de Mesquita Filho,” 15054-000, São José do Rio Preto, São Paulo, Brazil.

^b Laboratório de Materiais Funcionais Avançados (LaMFA), Departamento de Física, Universidade Federal do Ceará, 60455-900, Fortaleza, Ceará, Brazil.

^c Laboratoire MIO–Equipe CEM, Université de Toulon, CS 60584, 83041, CEDEX 9, Toulon, France.

***Corresponding author**

Name: Márcia Cristina Bisinoti

E-mail: marcia.bisinoti@unesp.br

Phone: +55 17 3221-2352

Address: Laboratório de Estudos em Ciências Ambientais, Departamento de Química e Ciências Ambientais, Instituto de Biociências, Letras e Ciências Exatas, Universidade Estadual Paulista “Júlio de Mesquita Filho”, Rua Cristóvão Colombo, 2265, 15054-000, São José do Rio Preto, São Paulo State, Brazil.

1
2
3
4
5
6
7
8
9
10
11
12
13
14
15
16
17
18
19
20
21
22
23
24
25

Abstract

Humic acids (HA) play an important role in the distribution, toxicity, and bioavailability of metals in the environment. Humic-like acids (HLA) that simulate geochemical processes can be prepared by NaOH aqueous extraction from hydrochars produced by hydrothermal carbonization (HTC). HLA can exhibit properties such as those found in HA from soils, which are known for their ability to interact with inorganic and organic compounds. The molecular characteristics of HLA and HA help to explain the relationship between their molecular features and their interaction with metallic species. The aim of this study is to assess the molecular features of HA extracted from *Terra Mulata* (TM) and HLA from hydrochars as well as their interaction with metals by using Cu(II) ions as a model. The results from ¹³C NMR, elemental analysis, FTIR, and UV-Vis showed that HA are composed mostly of aromatic structures and oxygenated functional groups, whereas HLA showed a mutual contribution of aromatic and aliphatic structures as main constituents. The interactions of HA and HLA with Cu(II) ions were evaluated through fluorescence quenching, in which the density of complexing sites per gram of carbon for interaction was higher for HLA than for HA. Furthermore, the HLA showed similar values for stability constants, and higher than those found for other types of HA in the literature. In addition, the average lifetime in both humic extracts appeared to be independent of the copper addition, indicating that the main mechanism of interaction was static quenching with a non-fluorescent ground-state complex formation. Therefore, the HLA showed the ability to interact with Cu(II) ions, which suggests that their application can provide a new approach for remediation of contaminated areas.

Keywords: hydrothermal carbonization, anthropogenic soils, complexation, fluorescence lifetime, soil remediation

26 **1. Introduction**

27 Metal pollution is a worldwide environmental issue in which human activity
28 plays a major role (Lesmana et al., 2009; Li et al., 2014). Unlike most organic
29 contaminants, metals are not biodegradable and can accumulate in living organisms,
30 thereby causing problems for both human health and the environment (Lesmana et al.,
31 2009). Some metals of great concern are cadmium, zinc, copper, and nickel (Li et al.,
32 2014; Tang et al., 2014). Among them, copper is important for cellular metabolism.
33 However, this element is highly toxic if swallowed at high concentrations and can cause
34 gastrointestinal problems, hair loss, weight loss, and even death (Andreazza et al., 2010;
35 Fu and Wang, 2011; Tang et al., 2014). Intensified industrial, agricultural, mining, and
36 urbanization activities are the main causes of copper contamination (Hladun et al., 2015;
37 MacKie et al., 2012). Therefore, research is needed to develop techniques for reducing
38 the concentrations of metals in contaminated soils.

39 It is widely accepted that soil fertility depends on the presence of nutrients and
40 organic matter (Stevenson, 1994). Humic substances (HS) are the main constituents of
41 soil organic matter and are formed from the remains of plant and animal degradation.
42 Humic acids (HA) are one of the components of HS. They represent the most
43 hydrophobic part and play important roles in soil fertility, water retention, plant growth
44 promotion, and interaction with organic and inorganic compounds (Bento et al., 2019;
45 Canellas and Façanha, 2004; Jindo et al., 2016). The bioavailability, distribution, and
46 toxicity of pollutants are affected by their interaction (He et al., 2016; Tang et al.,
47 2014); thus, the use of HA has gained attention for remediation (Piccolo et al., 2019).

48 Anthropogenic soils such as TM occur near the Amazon basin and are known
49 for exhibiting high fertility (Glaser et al., 2000; Oliveira et al., 2018). Such soils have
50 gained the attention of researchers who have attempted to reproduce their organic matter

51 by thermochemical methods of biomass conversion, such as pyrolysis and hydrothermal
52 carbonization (HTC). These methods use various biomass types to obtain a material
53 with the characteristics of TM.

54 The HTC process is a suitable biomass disposal method for the production of
55 carbon-based materials known as hydrochar. In addition, the process water (liquid
56 phase) is generated by this method. Some authors have proposed the use of this process
57 water as a hydrothermal medium in a new carbonization process (Kabadayi Catalkopru
58 et al., 2017; Stemann et al., 2013; Weiner et al., 2014) or for liquid fertilizer (Fregolente
59 et al., 2018).

60 Most HA used in the literature are extracted from soils, water, sediments, or peat
61 (Chen et al., 2015; Plaza et al., 2005; Zhrebtssov et al., 2015). The formation of these
62 environmental elements under natural conditions requires significant amounts of time
63 and involves several chemical and biological reactions that can last for years (Yang et
64 al., 2019a). However, the formation of HTC needs only hours (Melo et al., 2017; Silva
65 et al., 2017). Humic-like acids (HLA) are defined as extracts of different organic
66 materials that have not undergone the natural process of humification (Bento et al.,
67 2019; Jindo et al., 2016, 2019). Although there is not the natural humification process
68 that occurs in soils, HLA extracted from hydrochars might have characteristics similar
69 to those of natural HA extracted from anthropogenic soils, which are known as a model
70 of organic matter. Knowledge of the chemical structure of HLA is essential for
71 predicting their behavior and benefits in soil.

72 Because natural HA form complexes with metals (Stevenson, 1994), the study of
73 interaction between metallic ions and HLA is of significant value for predicting whether
74 HLA can assist in the complexation reactions if applied to the soil, and thus the metal
75 bioavailability. A variety of agents has been used for soil washing including

76 biosurfactants as well as synthetic agents such as ethylenediaminetetraacetic acid
77 (EDTA) (Mulligan et al., 2001, Mulligan, 2009). Despite the efficiency of these agents
78 in removing metals from soils, they cause environmental problems and are high in cost,
79 which justifies the need for more studies to develop new washing agents. In previous
80 research, a solution of HLA from manure compost biochar showed the remediation of
81 soils contaminated by multiple metals (Kulikowska et al., 2015); the same was shown
82 for HLA from composted sewage sludge (Piccolo et al., 2019). In addition, the potential
83 of HLA extracted from hydrochars produced with crude waste biomass was presented
84 (Yang et al., 2019a). In that case, HLA from hydrochars produced with by-products of
85 the sugarcane industry were shown to act in complexation reactions between metals and
86 active sites on the HLA surface.

87 The fluorescence excitation emission matrix (EEM) has gained prominence in
88 the characterization of organic matter and its interaction with metallic species (Elkins
89 and Nelson, 2002). The analytical potential of fluorescence EEM spectra coupled with
90 chemometric tools such as Parallel Factor Analysis (PARAFAC) has been successfully
91 realized for this type of analysis (Mounier et al., 2011; Nouhi et al., 2018; Stedmon and
92 Bro, 2008; Tadini et al., 2019; Yuan et al., 2015). Moreover, PARAFAC has also been
93 used in the characterization of dissolved organic matter (DOM) of biochars produced
94 with different biomass content (El-Naggar et al., 2020; Rajapaksha et al., 2019; Yang et
95 al., 2019b). Further, because different chemical species have different fluorescence
96 lifetimes, it is also possible to study organic matter–metal interaction through time-
97 resolved fluorescence (TRF), particularly in complex samples such as HA and HLA
98 (Nouhi et al., 2018).

99 Thus, the chemical characterization of HLA from hydrochars obtained with
100 sugarcane industry by-products was conducted, and the results were compared with that

101 of HA from TM. In addition, the interaction of HA and HLA with Cu(II) ions by
102 fluorescence quenching was studied to provide quantitative data on the complexation
103 capacity (CC), concentration of binding sites (CL), and conditional stability constant
104 (K). TRF as a complementary technique of fluorescence quenching was used to
105 investigate the interaction by measuring the fluorescence lifetime and its variation with
106 the addition of metal. Thus, the present study can provide a new perspective for
107 analyzing Cu(II)–HLA interactions and the potential of HLA as a complexing agent in
108 the remediation of soils polluted by metals.

109

110 **2. Materials and methods**

111 **2.1 *Terra Mulata* sampling**

112 Soil sampling was performed following the 2000 United States Environmental
113 Protection Agency (EPA) method (US EPA, 2000). For this study, three different areas
114 of TM were selected. The first TM soil was obtained from an open area region
115 containing native vegetation and low vegetation cover (TM I; 3°04'05.45" S and
116 58°33'51.11" W); the second was taken from a closed area region containing native
117 vegetation (TM II; 3°04'05.17" S and 58°34'11.68" W); and the third was collected near
118 cultivated areas (TM III; 3°03'59.15" S and 58°27'04.64" W). All areas are located near
119 Itacoatiara city in the Amazonas State (Brazil). (SISBio collection was authorized by
120 the Chico Mendes Institute for Biodiversity Conservation, n ° 50042 -2, and registered
121 in the National System for the Management of Genetic Heritage and Associated
122 Traditional Knowledge (SisGen), No. A0018C2.) Soil samples were collected from the
123 0 to 30 cm deep layer, air-dried, and subsequently sieved through a 2 mm mesh for
124 removal of plant debris and fragments.

125

126 **2.2 Hydrothermal carbonization and recarbonization process**

127 HTC was performed using vinasse and sugarcane bagasse, in which the vinasse
128 was used to produce the hydrothermal medium (Melo et al., 2017; Silva et al., 2017).
129 The HTC processes were conducted in a Teflon® closed reactor coated with stainless
130 steel. Each mixture (Table 1) was heated in a muffle furnace at 230 °C for 13 h. Then,
131 the reactor was cooled in an ice bath, and the suspension was filtered under vacuum
132 filtration to separate the hydrochar from the process water. The hydrochar was washed
133 with distilled water until constant pH was reached and was then dried at 50 °C until
134 constant mass was achieved. The process water generated in the HTC process was used
135 in the recarbonization process to produce the hydrothermal medium for sugarcane
136 bagasse carbonization. The subsequent steps after carbonization, i.e., filtration,
137 hydrochar washing, and drying, were the same.

138 **Table 1**

139 **2.3 Extraction of humic acids and humic-like acids**

140 The extractions were performed following the recommendations of the
141 International Humic Substances Society (IHSS) (Swift, 1996). HS were extracted from
142 TM at a proportion of 1:10 (soil:extractor). Thus, the extraction was conducted in 100 g
143 of soil to 1 L of solution (NaOH 0.1 mol L⁻¹) under nitrogen flow for 4 h. The solution
144 extracted was acidified with HCl (6 mol L⁻¹) to reach pH~1. Thus, HA were
145 precipitated, and fulvic acids remained in the supernatant. Subsequently, the HA were
146 separated by centrifugation, dialyzed using a Fisherbrand apparatus with a molecular
147 weight cut-off at 6,000–8,000 Da, and freeze-dried.

148 The method was modified for the extraction of humic-like substances (Jindo et al.,
149 2016). Those from hydrochars were extracted at a proportion of 1:10
150 (hydrochar:extractor) using NaOH (0.1 mol L⁻¹) under nitrogen flow for 4 h. This

151 procedure was repeated, with the same hydrochar portion until the final extract
152 (supernatant phase) showed a lighter color. HLA were obtained by the pH difference,
153 with HCl (6 mol L⁻¹) to pH~1, and was separated from the fulvic-like acids by
154 centrifugation. Finally, the extracts of HLA obtained from each extraction step were
155 combined, dialyzed, and freeze-dried.

156

157 **2.4 Characterization of humic acids and humic-like acids**

158 **2.4.1 Elemental analysis**

159 Elemental analyses were performed on solids using an elemental analyzer (2400
160 Series II CHNS/O, Perkin Elmer, Walther, Massachusetts, USA). The oxygen content
161 was determined according to the difference, i.e., O% = 100 - (C, H, N, S + ashes). The
162 ash content was determined in a muffle furnace at 750 °C for 4 h. The C, H, N, S, and O
163 contents were recalculated on an ash-free basis. The H/C, O/C, and C/N atomic ratios
164 were determined by elemental analysis (Giovanela et al., 2010; Stevenson, 1994).

165

166 **2.4.2 Infrared spectroscopy**

167 Infrared spectra were obtained using an attenuated total reflectance (ATR)-
168 coupled spectrophotometer (FTIR; Spectrum Two UATR, Perkin Elmer, Walther,
169 Massachusetts, USA). The solid material was placed directly on the ATR crystal and
170 was analyzed at a spectral range of 4000–400 cm⁻¹ with 20 scans and a resolution of 4
171 cm⁻¹.

172

173 **2.4.3 Ultraviolet–visible spectroscopy**

174 The ultraviolet-visible (UV–Vis) scanning spectra were obtained by employing a
175 UV–Vis spectrophotometer (UV-2600, Shimadzu, Japan) at a range of 200–700 nm. HA

176 and HLA solutions (10 mg L⁻¹) in total organic carbon (TOC; TOC-VCSN Shimadzu,
177 Japan) were diluted in 0.05 mol L⁻¹ of NaHCO₃ at pH 8. From the spectra, the ratios
178 E₄₆₅/E₆₆₅ (E4/E6) and E₂₇₀/E₄₀₇ (E2/E4) were calculated. These ratios have been used to
179 describe the degree of aromatic ring condensation and the presence of lignin derivatives,
180 respectively (Budziak et al., 2004; Canellas and Façanha, 2004).

181

182 **2.4.4 Solid-state ¹³C–CPMAS–NMR spectroscopy**

183 Solid-state ¹³C–cross-polarized magic angle spinning (CPMAS)–nuclear
184 magnetic resonance (NMR) characterization was performed by employing a Bruker
185 AVANCE 400 MHz spectrometer (Bruker, Billerica, Massachusetts, USA) equipped
186 with a magic angle spin (MAS) probe. A zircon cylindrical rotor with a diameter of 4.0
187 mm was packed with 80 mg of sample. The spectra were acquired by using a rotor
188 rotation frequency of 10 kHz, recycle time of 1 s, and 5,000 scans. The spectral areas
189 were integrated and divided into seven chemical shifts: C-alkyl (0–45 ppm), C-
190 methoxyl (45–60 ppm), O-alkyl-C (60–110 ppm), aryl-C (110–145 ppm), phenol-C
191 (145–160 ppm), carboxyl-C (160–190 ppm), and carbonyl-C (190–220 ppm).
192 According to the area integration, the aromaticity (ARM), alkyl (A/AO), and
193 hydrophobicity (HB/HI) indices were calculated. (Monda et al., 2018).

194

195 **2.5 Interaction of humic acids and humic-like acids with Cu(II)**

196 **2.5.1 Fluorescence quenching**

197 Studies involving interaction with Cu(II) ions were performed using 10 mg L⁻¹
198 of HA or HLA in a buffer medium with 0.1 mol L⁻¹ 4-(2-hydroxyethyl)-1-
199 piperazineethanesulfonic acid (HEPES) at pH 7.0. Titration experiments were
200 performed in 13 cuvettes for each HA or HLA sample with various concentrations of

201 Cu(II) ($\text{Cu}(\text{ClO}_4)_2 \cdot 6\text{H}_2\text{O}$), ranging from 0 mg L^{-1} to 11.2 mg L^{-1} . The equilibrium time
202 of 30 min was determined on the basis of changes observed in the fluorescence signal.
203 Fluorescence measurements were performed using a spectrofluorometer (F4500,
204 Hitachi, Santa Clara, California, USA) equipped with a 450 W xenon lamp. The spectra
205 were acquired in the scan ranges of 220–700 nm for emission and 220–500 nm for
206 excitation, with both slits fixed at 5 nm. The scan speed was set at $2,400 \text{ nm min}^{-1}$, and
207 the detector voltage was 700 V. The obtained EEM spectra were treated by using the
208 PARAFAC chemometric model. The number of components responsible for
209 fluorescence was defined by using the core consistency diagnostic (CORCONDIA)
210 (Mounier et al., 2011). The density of binding sites (CL) as well as the conditional
211 stability constant (K) were determined following the metal complexation model
212 proposed by Ryan and Weber (1982), as represented by



214 where L is a free complexing site, M is the free or uncomplexed metal, and ML is the
215 complex. Based on this reaction, the conditional stability constant can be calculated as

$$216 \quad K = [ML] / [M][L]. \quad (2)$$

217 Metal and complexing sites follow a mass balance in solution:

$$218 \quad CL = [ML] + [L], \quad (3)$$

$$219 \quad CM = [ML] + [M], \quad (4)$$

220 where CL and CM represent the total concentration of complexing sites and the metal in
221 the solution system, respectively.

222

223 **2.5.2 Time-resolved fluorescence**

224 Three samples were selected from the data obtained from the fluorescence
225 quenching experiment, i.e., three total copper concentrations for each HA and HLA

226 interaction. The first contained no concentration of copper (C_0), whereas $C_{0.7}$ and $C_{5.6}$
227 contained 0.7 mg L^{-1} and 5.6 mg L^{-1} , respectively. Prior to each measurement, the
228 prepared solution was bubbled with nitrogen for 10 min to prevent photodegradation.
229 TRF experiments were performed at 266 nm from the fourth harmonic generation from
230 a nanosecond laser Nd:YAG (Quanta-Ray INDI, Spectra Physic, Germany), and
231 excitation (1024 nm) occurred with a pulse width of 5 ns and a repetition of 20 Hz. Six
232 hundred spectra were accumulated at each time step of 0.2 ns with an optical fiber and
233 were detected by an intensified charge-coupled device (CCD) camera with a 35 ns gate
234 width. Data obtained by TRFS were corrected by energy fluctuation and were treated by
235 using a homemade MATLAB[®] program to obtain the spectral deconvolution and the
236 associated lifetime values.

237

238 **3. Results and discussion**

239 **3.1 Characterization of humic acids and humic-like acids**

240 Determining the molecular formula of HA and HLA is still a challenge;
241 however, elemental analysis can provide a general idea about their compositions. The
242 elemental analysis and UV–Vis ratios of soil HA and hydrochar HLA samples are
243 shown in Table 2. In general, HA and HLA showed carbon as the main constituent, at
244 36.6% to 62.2%, followed by oxygen, hydrogen, nitrogen, and sulfur. In addition, HLA
245 RHH_2SO_4 had the highest sulfur content of the samples. Regarding the carbon
246 percentage, the HLA samples showed higher values than did HA.

247 The O/C, H/C, and C/N atomic ratios (Table 2) based on elemental analysis,
248 have been used to describe the content of oxygenated groups in the molecules, the
249 degree of aromatic ring condensation, and the nitrogen content, respectively (Giovanela
250 et al., 2010; Stevenson, 1994). In general, HA showed higher O/C ratios than those of

251 HLA, suggesting a greater abundance of oxygen-containing functional groups
252 (Fukushima et al., 2014). The H/C ratio showed that HA, except for the TM II HA, have
253 higher condensation of aromatic rings than do HLA; lower C/N atomic ratios for HA
254 suggest more nitrogen-containing structures (F. Yang et al., 2019).

255 The UV–Vis spectra of HA have been previously described in the literature and
256 provide little structural information. Generally, however, the overall absorbance
257 decreases with increasing wavelength (Uyguner and Bekbolet, 2005). In this study, both
258 HA and HLA showed this behavior; the spectra are shown in the supplementary
259 material (Figure S1). For better interpretation of UV–Vis analysis, the absorbance ratios
260 at certain wavelengths were utilized. The E_{465}/E_{665} absorbance ratio is related to the
261 degree of condensation of aromatic rings. Values lower than 4 indicate compounds with
262 more condensed aromatic groups (Canellas and Façanha, 2004; Stevenson, 1994; He et
263 al., 2016). The E_{270}/E_{407} absorbance ratio refers to the presence of lignin derivatives, of
264 which the content is directly proportional to this value (Budziak et al., 2004). This ratio
265 might be indicative for organic matter studies because lignin is involved in the
266 formation of both soils and hydrochars. The obtained parameters are presented in Table
267 2.

268 HA showed a higher degree of aromatic condensation than HLA. Furthermore,
269 the lower number of compounds with lignin structures might be linked to greater
270 decomposition of organic matter.

271 **Table 2**

272 The FTIR spectra (Figure 1a and 1b) showed that both HA and HLA have
273 typical features of HS (Esteves et al., 2009; Fernandes et al., 2010; Giovanela et al.,
274 2010). In the 3500–3300 cm^{-1} region, larger bands were observed for HA. However, the
275 bands for HLA were more defined and might be related to N-H stretching of amines or

276 amides and O-H stretching of alcohols and phenols (Dick et al., 2003). The same result
277 was observed for the C-H stretching of aliphatic methyl and methylene groups near
278 2900 cm^{-1} . In the $1730\text{--}1710\text{ cm}^{-1}$ region, low intensity of C=O stretching of carboxylic
279 acids or ketones was found for HA (Figure 1a), and a slight shoulder was observed for
280 the HLA samples (Figure 1b) (Senesi et al., 2003). Bands in the $1620\text{--}1600\text{ cm}^{-1}$
281 regions were associated with aromatic C=C stretching (Stevenson, 1994). C-H bending
282 of CH_3 and deformation of CH_2 and CH_3 structures were observed in the $1420\text{--}1380\text{ cm}^{-1}$
283 region for HLA but not for HA. All spectra showed C-O-C stretching at approximately
284 $1250\text{--}1030\text{ cm}^{-1}$, likely resulting from polysaccharides; stretching in esters, alcohols,
285 and phenols was also observed. In addition, Si-O stretching bands were identified in the
286 $825\text{--}750\text{ cm}^{-1}$ region (Giovanela et al., 2010; Stevenson, 1994).

287 **Figure 1**

288 The ^{13}C -CPMAS-NMR spectra of HA and HLA are shown in Figure 2. Both
289 samples showed complex chemical compositions, with peaks related to aromatic and
290 aliphatic carbons, substituted or not by heteroatoms, and different intensities. The
291 following peaks were observed in all samples: $0\text{--}45\text{ ppm}$, attributed to the presence of
292 alkyl carbons of methyl and methylene groups; $45\text{--}60\text{ ppm}$ for carbons linked to
293 methoxyl groups and nitrogen compounds (C-N); $60\text{--}110\text{ ppm}$, indicating the presence
294 of oxygen-substituted carbons and alkyl groups (O-alkyl); $110\text{--}145\text{ ppm}$, attributed to
295 the presence of aromatic groups; and $145\text{--}160\text{ ppm}$ for substituted aromatic carbons,
296 $160\text{--}190\text{ ppm}$ for carbonyl groups, and $190\text{--}220\text{ ppm}$ for carboxylic groups in the
297 structures of HA and HLA (Mazzei and Piccolo, 2012; Monda et al., 2017; Spaccini and
298 Piccolo, 2009; Tadini et al., 2015).

299 Chemical shifts near 15 ppm were assigned to short-chain aliphatic structures,
300 whereas those at 30 ppm were assigned to long-chain aliphatic structures attributed to

301 lipid compounds, such as plant waxes and biopolyesters (Francioso et al., 2002; Monda
302 et al., 2017; Spaccini et al., 2019). These peaks were more intense in the HLA samples
303 (Figure 2). The peak at 54 ppm, related to the presence of methoxyl carbons in both
304 guaiacil and syringyl units of lignin fragments, as well as C α of oligo- and polypeptides
305 (Monda et al., 2017), was present for both HA and HLA except in those in which
306 sulfuric acid was used as an additive (Figure 2).

307 The peaks in the 71–74 ppm range were more evident in HA and are typical of
308 O-akyl-C in mono and polysaccharides, in which the centered peak at 72 ppm is
309 attributed to the overlapping of carbon numbers 2, 3, and 5 in the pyranosidic cellulose
310 and hemicellulose structures, referred to as C-2, C-3, and C-5, respectively (Monda et
311 al., 2017; Spaccini and Piccolo, 2009). Unsubstituted aromatic carbons were responsible
312 for the intense signal at 130 ppm (Monda et al., 2017) in the HA and HLA structures,
313 whereas their analogs containing -OH, -OCH₃, and -NH₂ groups were found in the 145–
314 160 ppm region. The signal at 174 ppm corresponds to carboxylic acids, and the low
315 signal at 190–220 ppm refers to carbonyl groups of ketones, amides, and aldehyde (Mao
316 et al., 2011) in the HA and HLA, as shown in Figure 2.

317 **Figure 2**

318 By employing spectral integration, it is possible to estimate the distribution of
319 carbons in the HA and HLA structures as well as some indices such as A/AO, ARM,
320 and HB/HI, as shown in Table 3. These indices are related to the biochemical stability
321 of different organic compounds. The HA showed aromatic compounds as the main
322 constituents, whereas HLA showed the presence of aromatic and aliphatic carbons
323 (Table 3). The ARM index was similar for both materials. Higher HB/HI index values
324 indicate the incorporation of hydrophobic moieties in HLA (Bento et al., 2019).
325 Furthermore, the natural HA were more hydrophilic than those HLA obtained from

326 HTC, which is indicated by the decrease in the A/OA index (Table 3). All of these
327 factors, such as presence or absence, greater incorporation of functional groups or not in
328 humic and humic-like acids, influence the binding properties with metal ions.

329 **Table 3**

330

331 **3.2 Interaction of humic acids and humic-like acids with Cu(II)**

332 **3.2.1 Fluorescence quenching**

333 The interactions of HA and HLA with Cu(II) ions were evaluated by
334 fluorescence quenching; the concentration of each humic extract was 10 mg L⁻¹. Other
335 authors have used this concentration value of humic extract in experiments for the same
336 purpose: to avoid inner filters (Guo et al., 2015; Yuan et al., 2015). The quenching
337 results were combined with the PARAFAC multivariate statistical tool, in which the
338 complex signal of the fluorescence spectra was decomposed into simple and
339 independent components.

340 Thus, a three-component model was found for HA quenching experiments with
341 a good CORCONDIA value (94.75%). The components are shown in Figure 3.
342 Component 1 (Figure 3a) had a main peak at [λ_{Ex} 300 nm/ λ_{Em} 475 nm], which is typical
343 of humic-like substances. Component 2 (Figure 3b) had a secondary peak at [λ_{Ex} 275
344 nm/ λ_{Em} 530 nm], which is associated with low-energy peaks known to be typically
345 linked to terrestrial HA (Matthews et al., 1996; Stedmon et al., 2003), and a main peak
346 at [λ_{Ex} 475 nm/ λ_{Em} 530 nm], which is typical of lignin-derived terrestrial HA. In
347 addition, component 1 showed a blue shift for fluorescence emission intensity, whereas
348 component 2 demonstrated a red shift, characterizing the presence of simple and
349 complex structures, respectively (Senesi et al., 2003). Conversely, component 3 (Figure
350 3c) showed no variation in its contribution during the quenching experiments, which is

351 likely related to a noise factor. Therefore, this component was not considered in the
352 discussion.

353 A three-component model was also found for the interaction with HLA, with a
354 CORCONDIA value of 97.46%; these components are also shown in Figure 3.
355 Component 1 (Figure 3d) showed a main and a secondary peak at [λ_{Ex} 260 nm/ λ_{Em} 425
356 nm] and [λ_{Ex} 340 nm/ λ_{Em} 425 nm], respectively. Both components are characteristic of
357 humic substances from terrestrial environments (Coble, 1996; Matthews et al., 1996;
358 Stedmon et al., 2003). Component 2 (Figure 3e) had a main peak at [λ_{Ex} 275 nm/ λ_{Em}
359 510 nm] and a secondary peak at [λ_{Ex} 400 nm/ λ_{Em} 510 nm]. The main peak was
360 classified as typically humic-like, and the secondary peak refers to soil fulvic acid.
361 Component 3 (Figure 3f) showed no fluorescence variation; therefore, similar to that for
362 HA, it was not considered in the discussion.

363 **Figure 3**

364 It is possible to obtain the fluorescence contribution of each component in the
365 sample, known as the score, depending on the metal addition. The initial humic extracts
366 were considered as 100%, and the contribution decreased with the addition of metal.
367 Figure 4a shows the scores of components 1 and 2 regarding the interaction of TM I HA
368 with Cu(II) ions, and Figure 4b shows those regarding the interaction of HH₂SO₄ HLA.
369 All three HA samples showed similar behavior; additional graphs are given in the
370 supplementary material (Figure S2). The four HLA samples also showed similarly
371 behavior, as shown in the supplementary material (Figure S3).

372 **Figure 4**

373 The fluorescence quenching curve for the first component of HA and Cu(II)
374 (Figure 4a) showed a fluorescence intensity decay of approximately 85.6%, and the
375 second component had a value of 92.5%. This significant decay in fluorescence

376 contribution is attributed to the formation of a complex in which the fluorescence
377 quantum yield changed (Mounier et al., 2011; Tadini et al., 2019). Moreover, the
378 interaction with Cu(II) was shown to influence the optical properties of organic matter.
379 For the interaction between HLA and Cu(II) (Figure 4b), the fluorescence intensity
380 decay for the first component remained at approximately 67.3%, whereas that for the
381 second was approximately 58.2%. The decrease in fluorescence intensity of the HA
382 components appeared at the first concentrations of Cu(II). For the HLA components, an
383 increase in copper concentration was necessary for better visualization of the quenching
384 phenomenon.

385 Optimization of the data using the 1:1 (ligand:metal) complexation model
386 proposed by Ryan and Weber (1982) enables evaluation of the equilibrium parameters,
387 particularly CL and K, of which CL is the concentration of binding sites capable of
388 forming a complex and K is the conditional stability constant of the complex formed.

389 The equilibrium parameters for the HA and HLA experiments, including CL, log
390 K, CC, and the bias values, are given in Table 4. To evaluate the 1:1 complexation
391 model, bias was used as an optimization parameter. Bias is the sum of the absolute
392 value of the difference between the experimental and calculated fluorescence logarithm
393 intensity. In this study, the bias values ranged from 0.27 to 4.18, which are lower than
394 those found in the literature (Tadini et al., 2019). Therefore, the experimental data fit
395 well in the theoretical model (Table 4). The titration curves of the theoretical and
396 experimental values for components 1 and 2 of HA and components 1 and 2 of HLA
397 with Cu(II) can be found in the supplementary material (Figures S4 and S5).

398 **Table 4**

399 For HA components 1 and 2, the log K values remained in the ranges of 5.30–
400 5.41 and 5.58–5.60, respectively; for HLA components 1 and 2, these values were in the

401 ranges of 4.88–4.90 and 5.06–5.09, respectively. The HA components showed higher
402 values for log K and both blue and red shifts in the fluorescence emission wavelengths.
403 In addition, the fluorophores exhibited different chemical structures and compounds
404 with good binding capacities, which is confirmed by Figure 3a, b. The HLA
405 components showed similar values for log K compared with HA and values either
406 similar to or higher than those found in the literature for other types of HA (Fuentes et
407 al., 2013; Plaza et al., 2005; Tadini et al., 2019). Blue and red shifts were also observed
408 (Figure 3d, e); therefore, the fluorophores have different chemical structures and are
409 weakly bonded compared to HA.

410 It is noteworthy that TM, which occurs in the Amazon, is different from
411 common soils and has high fertility because of the carbon stock and long-term nutrients.
412 This fact was demonstrated by good interaction with the metal ion (log K 5.30–5.60).
413 HLA showed higher log K values than those found in Spodosols, which also occur in
414 the Amazon region (log K 3.79–5.32) (Tadini et al., 2019), or peat and leonardite (log K
415 4.58–5.10) (Fuentes et al., 2013). This indicates that the organic matter extracted from
416 hydrochars can also interact satisfactorily with Cu(II) ions to form complexes.
417 Additionally, by using the CL values, it was also possible to determine the CC for all
418 components 1 and 2 from HA and HLA. This parameter was obtained by dividing the
419 CL values by the carbon content. CC represents the concentration of binding sites per
420 gram of carbon available to interact with Cu(II) ions. Table 4 also shows the CC values
421 for HA and HLA components 1 and 2.

422 Both HLA components 1 and 2 showed higher concentrations of binding sites
423 per gram of carbon for interaction with Cu(II) ions than those of HA; and the highest
424 value was observed for RHH₂SO₄ HLA. Regarding log K, the CC values were also
425 higher than those found in the literature for HA from soils, peat, or leonardite (Fuentes

426 et al., 2013; Plaza et al., 2005; Tadini et al., 2019). Tadini et al. (2019) determined the
427 CC of components by fluorescence quenching for HA extracted from Amazonian
428 Spodosols with Cu(II) ions and found CC values ranging from 0.01–0.13 mmol of Cu g⁻¹
429 ¹³C. The values found in this study for HA extracted from TM were higher, indicating
430 both a larger amount of complexing sites and an affinity of organic matter with the
431 metallic ion. The same result was observed for HLA, indicating that if applied to the
432 soil, it could help in the complexation reactions.

433 Previous research indicates that the high stability constants of HA are associated
434 with increased oxygen-containing groups such as -COOH and -OH as well as π - π bonds
435 in the C=C of aromatic rings (Guo et al., 2012, 2015). These functional groups were
436 observed for HA and HLA by using both FTIR and ¹³C NMR techniques. The results
437 show that the predominance of conjugate and aromatic structures as well as oxygen-
438 containing groups are responsible for HA complexation, and for HLA, both aromatic
439 and aliphatic groups are responsible. Pearson established the concept of chemical
440 bonding regarding the affinity of different metals to different ligands (Pearson, 1963). It
441 was reported that chemical species can be classified as “hard” and “soft” or “borderline”
442 acids and bases and that the concepts of “hardness” and “softness” can help to interpret
443 the mechanism of complexation. Soft acids tend to have preferential interaction by soft
444 bases, whereas hard acids tend to bind with hard bases; borderline acids form
445 considerably stable bonds with both hard and soft bases, although it is sometimes
446 difficult to determine the preferential order for bond formation. These concepts partly
447 explain the stability of chemical compounds (Pearson, 1963).

448 As observed in the ¹³C NMR spectra and in the H/C, O/C, and C/N atomic
449 ratios, HA and HLA showed similar ARM, although HA showed a higher percentage of
450 oxygenated groups and nitrogen in its structure. The Cu(II) ion used in this study is a

451 borderline acid and interacts with both hard bases such as oxygen and soft bases such as
452 nitrogen; thus, HA had a stronger interaction with Cu(II) because of their molecular
453 structures. Lu and Allen (2002) found that the interaction of DOM with Cu(II) ions is
454 attributed mostly to phenol OH groups, and Hernández (2006) showed a positive and
455 significant correlation with carboxylic acid and phenols. Moreover, the presence of
456 large amounts of functional groups and π - π bonds of aromatic rings should confer a
457 greater complexation capacity for HA from TM; however, this did not occur potentially
458 owing to the different molecular arrangements. Further, it is possible that the functional
459 groups and aromatic carbons in HA structures were already occupied by another metal
460 or more condensed aromatic rings. All of these factors can affect the behavior of Cu(II)
461 ions in both soils and hydrochar extracts. Conversely, HLA showed more binding sites
462 available for interaction considering the amount of carbon in the sample, and thus
463 greater complexation capacity.

464

465 **3.2.2 Time-resolved fluorescence**

466 In addition, fluorescence quenching can be induced by two mechanisms. The first
467 is dynamic quenching, which is caused by collision with a quencher and occurs during
468 the lifetime of the excited state, affecting the fluorescence lifetime. The second is static
469 quenching, which occurs when a ground-state non-fluorescent complex is formed, and
470 the lifetimes of the fluorescent ligand and complex are unaffected (Lakowics, 1999).
471 Therefore, TRF is the best method for distinguishing whether static or dynamic
472 quenching occurs during the interaction of organic matter with copper.

473 Figure 5a and 5b show the fluorescence average lifetime distribution of HA and
474 HLA complexes with copper, respectively. The deconvolution of TRF results in the HA
475 complexes show that the decay was mono-exponential (τ_1) decay containing only one

476 lifetime. The average lifetime values observed were shorter, at approximately 5–6 ns,
477 which is associated with the simple structure of HA. This average lifetime can be
478 attributed to component 1 (Figure 3a) observed in PARAFAC. The average lifetime of
479 component 2, with emission at 530 nm (Figure 3b) did not appear in the results because
480 the emission spectra in TRF reached only 510 nm owing to laser leakage at 532 nm.

481 The best fit for HLA complexes showed a bi-exponential decay (τ_1 and τ_2), the
482 average lifetimes of which were approximately 4 ns and 14 ns, respectively. These
483 results fit well with the PARAFAC for HLA, which showed two components, one with
484 a simple structure (component 1) and the other with a complex structure (component 2),
485 reflecting lower and higher lifetimes, respectively. The first average lifetime τ_1 was
486 almost the same as that for HA (Figure 3d). Lifetime τ_2 can be associated with
487 component 2 (Figure 3e), which has a more complex fluorophore structure.

488 **Figure 5**

489 The average lifetime values were determined to be independent of the copper
490 concentration for HA and HLA interaction (Figure 5). This suggests that the mechanism
491 of Cu(II) quenching by fluorescence occurs with a non-fluorescent ground-state
492 complex, i.e., the complexation occurs by static quenching. Nouhi (2018) also reported
493 static quenching and similar lifetime values for interaction between Cu(II) and Eu(III)
494 with HA extracted from the Saint Lawrence Estuary in Canada (Nouhi, 2018).

495 In summary, this study demonstrated the potential of fluorescence quenching
496 and TRF for evaluating the interaction between metallic species and organic matter,
497 which provides insight into the interaction mechanism. No previous studies related to
498 fluorescence quenching and lifetime measurements of HA extracted from Amazonian
499 TM and HLA from hydrochars with metallic species are available for comparison with
500 the results achieved here.

501

502 **4. Conclusion**

503 HLA were obtained by NaOH aqueous solution extraction from hydrochar
504 produced by the HTC process using sugarcane industry by-products. These HLA
505 showed greater complexation capacity with Cu(II) ions than the HA extracted from TM.
506 In addition, similar values for stability constants for both HA and HLA were observed.
507 The interaction with Cu(II) in HLA occurs by both aromatic and aliphatic moieties,
508 showing that π - π interaction and oxygen groups are not the only factors that play
509 important roles in the CC. Furthermore, the TRF for the interaction of metallic species
510 and organic matter showed that the main interaction mechanism was static quenching.
511 These results show that HLA extracted from hydrochars can be an efficient approach for
512 interacting with metals and can be a new tool for remediating areas contaminated by
513 metals.

514

515 **Acknowledgments**

516 This work was supported by the São Paulo Research Foundation (FAPESP)
517 (grants 15/22954-1, 17/26718-6, and 18/15733-7). J.V.S acknowledges a scholarship
518 from FAPESP (grants 17/05408-9 and 18/09914-9). O.P.F acknowledges financial
519 support from FUNCAP (PRONEX PR2-0101-00006.01.00/15). The authors thank Dr.
520 Maurício Boscolo for offering assistance with the FTIR analysis (process 2017/13230-
521 5) and Dr. Isabella Constatino and Dr. Fabiana Paschoal for their assistance with soil
522 sampling.

523

524 **References**

525 Andreatza, R., Okeke, B.C., Lambais, M.R., Bortolon, L., de Melo, G.W.B., de Oliveira

526 Camargo, F.A., 2010. Bacterial stimulation of copper phytoaccumulation by
527 bioaugmentation with rhizosphere bacteria. *Chemosphere* 81, 1149–1154.
528 <https://doi.org/10.1016/j.chemosphere.2010.09.047>

529 Bento, L. R.; Melo, C. A.; Ferreira, O. P.; Moreira, A. B.; Mounier, S.; Piccolo, A.;
530 Spaccini, R.; Bisinoti, M.C., 2020. Humic extracts of hydrochar and Amazonian
531 Dark Earth: Molecular characteristics and effects on maize seed germination. *Sci.*
532 *Total Environ.* <https://doi.org/10.1016/j.scitotenv.2019.135000>

533 Bento, L.R., Melo, C.A., Ferreira, O.P., Moreira, B., Mounier, S., Piccolo, A., Spaccini,
534 R., Bisinoti, M.C., 2019. Humic extracts of hydrochar and Amazonian Dark Earth:
535 Molecular characteristics and effects on maize seed germination. *Sci. Total*
536 *Environ.* 135000. <https://doi.org/10.1016/j.scitotenv.2019.135000>

537 Budziak, C.R., Maia, C.M.B.F., Mangrich, A.S., 2004. Transformações químicas da
538 matéria orgânica durante a compostagem de resíduos da indústria madeireira.
539 *Quim. Nova* 27, 399–403. <https://doi.org/10.1590/S0100-40422004000300007>

540 Canellas, L.P., Façanha, A.R., 2004. Chemical nature of soil humified fractions and
541 their bioactivity. *Pesqui. Agropecu. Bras.* 39, 233–240.
542 <https://doi.org/10.1590/S0100-204X2004000300005>

543 Chen, J., Chen, H., Zhang, X.W., Lei, K., Kenny, J.E., 2015. Combination of a Copper-
544 Ion Selective Electrode and Fluorometric Titration for the Determination of
545 Copper(II) Ion Conditional Stability Constants of Humic Substances. *Acta radiol.*
546 56, 1293–1302. <https://doi.org/10.1366/14-07835>

547 Coble, P.G., 1996. Characterization of marine and terrestrial DOM in the seawater using
548 exciting-emission matrix. *Mar. Chem.* 51, 325–346. [https://doi.org/10.1016/0304-](https://doi.org/10.1016/0304-4203(95)00062-3)
549 [4203\(95\)00062-3](https://doi.org/10.1016/0304-4203(95)00062-3)

550 Dick, D. P.; Santos, J. H. Z.; Ferranti, E.M., 2003. Chemical Characterization and
551 Infrared Spectroscopy of Soil Organic Matter From Two Southern Brazilian Soils (
552 1). Rev. Bras. Cienc. do Solo 27, 29–39. [https://doi.org/10.1590/S0100-](https://doi.org/10.1590/S0100-06832003000100004)
553 06832003000100004

554 El-Naggar, A., Lee, M.H., Hur, J., Lee, Y.H., Igalavithana, A.D., Shaheen, S.M., Ryu,
555 C., Rinklebe, J., Tsang, D.C.W., Ok, Y.S., 2020. Biochar-induced metal
556 immobilization and soil biogeochemical process: An integrated mechanistic
557 approach. Sci. Total Environ. 698, 134112.
558 <https://doi.org/10.1016/j.scitotenv.2019.134112>

559 Elkins, K.M., Nelson, D.J., 2002. Spectroscopic approaches to the study of the
560 interaction of aluminum with humic substances. Coord. Chem. Rev. 228, 205–225.
561 [https://doi.org/10.1016/S0010-8545\(02\)00040-1](https://doi.org/10.1016/S0010-8545(02)00040-1)

562 Esteves, V.I., Otero, M., Duarte, A.C., 2009. Comparative characterization of humic
563 substances from the open ocean, estuarine water and fresh water. Org. Geochem.
564 40, 942–950. <https://doi.org/10.1016/j.orggeochem.2009.06.006>

565 Fernandes, A.N., Giovanela, M., Esteves, V.I., Sierra, M.M. de S., 2010. Elemental and
566 spectral properties of peat and soil samples and their respective humic substances.
567 J. Mol. Struct. 971, 33–38. <https://doi.org/10.1016/j.molstruc.2010.02.069>

568 Francioso, O., Sánchez-Cortés, S., Casarini, D., Garcia-Ramos, J. V., Ciavatta, C.,
569 Gessa, C., 2002. Spectroscopic study of humic acids fractionated by means of
570 tangential ultrafiltration. J. Mol. Struct. 609, 137–147.
571 [https://doi.org/10.1016/S0022-2860\(01\)00971-1](https://doi.org/10.1016/S0022-2860(01)00971-1)

572 Fregolente, L.G., Miguel, T.B.A.R., de Castro Miguel, E., de Almeida Melo, C.,
573 Moreira, A.B., Ferreira, O.P., Bisinoti, M.C., 2018. Toxicity evaluation of process

574 water from hydrothermal carbonization of sugarcane industry by-products.
575 Environ. Sci. Pollut. Res. 1–11. <https://doi.org/10.1007/s11356-018-1771-2>

576 Fu, F., Wang, Q., 2011. Removal of heavy metal ions from wastewaters: A review. J.
577 Environ. Manage. 92, 407–418. <https://doi.org/10.1016/j.jenvman.2010.11.011>

578 Fuentes, M., Olaetxea, M., Baigorri, R., Zamarreño, A.M., Etienne, P., Laîné, P., Ourry,
579 A., Yvin, J.C., Garcia-Mina, J.M., 2013. Main binding sites involved in Fe(III) and
580 Cu(II) complexation in humic-based structures. J. Geochemical Explor. 129, 14–
581 17. <https://doi.org/10.1016/j.gexplo.2012.12.015>

582 Fukushima, M., Okabe, R., Nishimoto, R., Fukuchi, S., Sato, T., Terashima, M., 2014.
583 Adsorption of pentachlorophenol to a humin-like substance-bentonite complex
584 prepared by polycondensation reactions of humic precursors. Appl. Clay Sci. 87,
585 136–141. <https://doi.org/10.1016/j.clay.2013.10.022>

586 Giovanela, M., Crespo, J.S., Antunes, M., Adamatti, D.S., Fernandes, A.N., Barison, A.,
587 Da Silva, C.W.P., Guégan, R., Motelica-Heino, M., Sierra, M.M.D., 2010.
588 Chemical and spectroscopic characterization of humic acids extracted from the
589 bottom sediments of a Brazilian subtropical microbasin. J. Mol. Struct. 981, 111–
590 119. <https://doi.org/10.1016/j.molstruc.2010.07.038>

591 Glaser, B., Balashov, E., Haumaier, L., Guggenberger, G., Zech, W., 2000. Black
592 carbon in density fractions of anthropogenic soils of the Brazilian Amazon region.
593 Org. Geochem. 31. [https://doi.org/10.1016/S0146-6380\(00\)00044-9](https://doi.org/10.1016/S0146-6380(00)00044-9)

594 Guo, X., Jiang, J., Xi, B., He, X., Zhang, H., Deng, Y., 2012. Study on the spectral and
595 Cu (II) binding characteristics of DOM leached from soils and lake sediments in
596 the Hetao region. Environ. Sci. Pollut. Res. 19, 2079–2087.
597 <https://doi.org/10.1007/s11356-011-0704-0>

598 Guo, X. jing, Zhu, N. min, Chen, L., Yuan, D. hai, He, L. sheng, 2015. Characterizing
599 the fluorescent properties and copper complexation of dissolved organic matter in
600 saline-alkali soils using fluorescence excitation-emission matrix and parallel factor
601 analysis. *J. Soils Sediments* 15, 1473–1482. [https://doi.org/10.1007/s11368-015-](https://doi.org/10.1007/s11368-015-1113-7)
602 1113-7

603 He, E., Lü, C., He, J., Zhao, B., Wang, J., Zhang, R., Ding, T., 2016. Binding
604 characteristics of Cu²⁺ to natural humic acid fractions sequentially extracted from
605 the lake sediments. *Environ. Sci. Pollut. Res.* 23, 22667–22677.
606 <https://doi.org/10.1007/s11356-016-7487-2>

607 Hernández, D., Plaza, C., Senesi, N., Polo, A., 2006. Detection of Copper(II) and
608 zinc(II) binding to humic acids from pig slurry and amended soils by fluorescence
609 spectroscopy. *Environ. Pollut.* 143, 212–220.
610 <https://doi.org/10.1016/j.envpol.2005.11.038>

611 Hladun, K.R., Parker, D.R., Trumble, J.T., 2015. Cadmium, Copper, and Lead
612 Accumulation and Bioconcentration in the Vegetative and Reproductive Organs of
613 *Raphanus sativus*: Implications for Plant Performance and Pollination. *J. Chem.*
614 *Ecol.* 41, 386–395. <https://doi.org/10.1007/s10886-015-0569-7>

615 Jindo, K., Sánchez-Monedero, M.A., Matsumoto, K., Sonoki, T., 2019. The efficiency
616 of a low dose of biochar in enhancing the aromaticity of humic-like substance
617 extracted from poultry manure compost. *Agronomy* 9, 1–10.
618 <https://doi.org/10.3390/agronomy9050248>

619 Jindo, K., Sonoki, T., Matsumoto, K., Canellas, L., Roig, A., Sanchez-Monedero, M.A.,
620 2016. Influence of biochar addition on the humic substances of composting
621 manures. *Waste Manag.* 49, 545–552.

622 <https://doi.org/10.1016/j.wasman.2016.01.007>

623 Kabadayi Catalkopru, A., Kantarli, I.C., Yanik, J., 2017. Effects of spent liquor
624 recirculation in hydrothermal carbonization. *Bioresour. Technol.* 226, 89–93.
625 <https://doi.org/10.1016/j.biortech.2016.12.015>

626 Kulikowska, D., Gusiatin, Z.M., Bułkowska, K., Klik, B., 2015. Feasibility of using
627 humic substances from compost to remove heavy metals (Cd, Cu, Ni, Pb, Zn) from
628 contaminated soil aged for different periods of time. *J. Hazard. Mater.* 300, 882–
629 891. <https://doi.org/10.1016/j.jhazmat.2015.08.022>

630 Lakowics, J.R., 1999. Principles of fluorescence spectroscopy, 2nd ed. New York:
631 Kluwer Academic/ Plenum Publisher.

632 Lesmana, S.O., Febriana, N., Soetaredjo, F.E., Sunarso, J., Ismadji, S., 2009. Studies on
633 potential applications of biomass for the separation of heavy metals from water and
634 wastewater. *Biochem. Eng. J.* 44, 19–41. <https://doi.org/10.1016/j.bej.2008.12.009>

635 Li, Z., Ma, Z., van der Kuijp, T.J., Yuan, Z., Huang, L., 2014. A review of soil heavy
636 metal pollution from mines in China: Pollution and health risk assessment. *Sci.*
637 *Total Environ.* 468–469, 843–853. <https://doi.org/10.1016/j.scitotenv.2013.08.090>

638 Lu, Y., Allen, H.E., 2002. Characterization of copper complexation with natural
639 dissolved organic matter (DOM) - Link to acidic moieties of DOM and
640 competition by Ca and Mg. *Water Res.* 36, 5083–5101.
641 [https://doi.org/10.1016/S0043-1354\(02\)00240-3](https://doi.org/10.1016/S0043-1354(02)00240-3)

642 MacKie, K.A., Müller, T., Kandeler, E., 2012. Remediation of copper in vineyards - A
643 mini review. *Environ. Pollut.* 167, 16–26.
644 <https://doi.org/10.1016/j.envpol.2012.03.023>

645 Mao, J., Chen, N., Cao, X., 2011. Characterization of humic substances by advanced
646 solid state NMR spectroscopy: Demonstration of a systematic approach. *Org.*
647 *Geochem.* 42, 891–902. <https://doi.org/10.1016/j.orggeochem.2011.03.023>

648 Matthews, B.J.H., Jones, A.C., Theodorou, N.K., Tudhope, A.W., 1996. Excitation-
649 emission-matrix fluorescence spectroscopy applied to humic acid bands in coral
650 reefs. *Mar. Chem.* 55, 317–332. [https://doi.org/10.1016/S0304-4203\(96\)00039-4](https://doi.org/10.1016/S0304-4203(96)00039-4)

651 Mazzei, P., Piccolo, A., 2012. Quantitative evaluation of noncovalent interactions
652 between glyphosate and dissolved humic substances by NMR spectroscopy.
653 *Environ. Sci. Technol.* 46, 5939–5946. <https://doi.org/10.1021/es300265a>

654 Melo, C.A., Junior, F.H.S., Bisinoti, M.C., Moreira, A.B., Ferreira, O.P., 2017.
655 Transforming sugarcane bagasse and vinasse wastes into hydrochar in the presence
656 of phosphoric acid: an evaluation of nutrient contents and structural properties.
657 *Waste and Biomass Valorization* 1139–1151. [https://doi.org/10.1007/s12649-016-](https://doi.org/10.1007/s12649-016-9664-4)
658 [9664-4](https://doi.org/10.1007/s12649-016-9664-4)

659 Monda, H., Cozzolino, V., Vinci, G., Drosos, M., Savy, D., Piccolo, A., 2018.
660 Molecular composition of the Humeome extracted from different green composts
661 and their biostimulation on early growth of maize. *Plant Soil* 429, 407–424.
662 <https://doi.org/10.1007/s11104-018-3642-5>

663 Monda, H., Cozzolino, V., Vinci, G., Spaccini, R., Piccolo, A., 2017. Molecular
664 characteristics of water-extractable organic matter from different composted
665 biomasses and their effects on seed germination and early growth of maize. *Sci.*
666 *Total Environ.* 590–591, 40–49. <https://doi.org/10.1016/j.scitotenv.2017.03.026>

667 Mounier, S., Zhao, H., Garnier, C., Redon, R., 2011. Copper complexing properties of
668 dissolved organic matter: PARAFAC treatment of fluorescence quenching.

669 Biogeochemistry 106, 107–116. <https://doi.org/10.1007/s10533-010-9486-6>

670 Mulligan, C.N., 2009. Recent advances in the environmental applications of
671 biosurfactants. *Curr. Opin. Colloid Interface Sci.* 14, 372–378.
672 <https://doi.org/10.1016/j.cocis.2009.06.005>

673 Mulligan, C.N., Yong, R.N., Gibbs, B.F., 2001. Heavy metal removal from sediments
674 by biosurfactants. *J. Hazard. Mater.* 85, 111–125. [https://doi.org/10.1016/S0304-](https://doi.org/10.1016/S0304-3894(01)00224-2)
675 [3894\(01\)00224-2](https://doi.org/10.1016/S0304-3894(01)00224-2)

676 Nouhi, A., 2018. Caractérisation Spectrale et Temporelle par Quenching de
677 Fluorescence des Interactions Matière Organique-Eléments Métalliques. Université
678 de Toulon.

679 Nouhi, A., Hajjoul, H., Redon, R., Gagné, J.P., Mounier, S., 2018. Time-resolved laser
680 fluorescence spectroscopy of organic ligands by europium: Fluorescence
681 quenching and lifetime properties. *Spectrochim. Acta - Part A Mol. Biomol.*
682 *Spectrosc.* 193, 219–225. <https://doi.org/10.1016/j.saa.2017.12.028>

683 Oliveira, N.C., Paschoal, A.R., Paula, R.J., Constantino, I.C., Bisinoti, M.C., Moreira,
684 A.B., Fregolente, L.G., Santana, A.M., Sousa, F.A., Ferreira, O.P., Paula, A.J.,
685 2018. Morphological analysis of soil particles at multiple length-scale reveals
686 nutrient stocks of Amazonian Anthrosols. *Geoderma* 311, 58–66.
687 <https://doi.org/10.1016/j.geoderma.2017.09.034>

688 Pearson, R.G., 1963. Hard and Soft Acids and Bases. *J. Am. Chem. Soc.* 85, 3533–
689 3539. <https://doi.org/10.1021/ja00905a001>

690 Piccolo, A., Spaccini, R., De Martino, A., Scognamiglio, F., di Meo, V., 2019. Soil
691 washing with solutions of humic substances from manure compost removes heavy

692 metal contaminants as a function of humic molecular composition. *Chemosphere*
693 225, 150–156. <https://doi.org/10.1016/j.chemosphere.2019.03.019>

694 Plaza, C., D’Orazio, V., Senesi, N., 2005. Copper(II) complexation of humic acids from
695 the first generation of EUROSOLS by total luminescence spectroscopy.
696 *Geoderma* 125, 177–186. <https://doi.org/10.1016/j.geoderma.2004.07.012>

697 Rajapaksha, A.U., Ok, Y.S., El-Naggar, A., Kim, H., Song, F., Kang, S., Tsang, Y.F.,
698 2019. Dissolved organic matter characterization of biochars produced from
699 different feedstock materials. *J. Environ. Manage.* 233, 393–399.
700 <https://doi.org/10.1016/j.jenvman.2018.12.069>

701 Ryan, D.K., Weber, J.H., 1982. Fluorescence Quenching Titration for Determination of
702 Complexing Capacities and Stability Constants of Fulvic Acid. *Anal. Chem.* 54,
703 986–990. <https://doi.org/10.1021/ac00243a033>

704 Senesi, N., D’Orazio, V., Ricca, G., 2003. Humic acids in the first generation of
705 EUROSOLS. *Geoderma* 116, 325–344. [https://doi.org/10.1016/S0016-](https://doi.org/10.1016/S0016-7061(03)00107-1)
706 [7061\(03\)00107-1](https://doi.org/10.1016/S0016-7061(03)00107-1)

707 Silva, C.C., Melo, C.A., Soares Junior, F.H., Moreira, A.B., Ferreira, O.P., Bisinoti,
708 M.C., 2017. Effect of the reaction medium on the immobilization of nutrients in
709 hydrochars obtained using sugarcane industry residues. *Bioresour. Technol.* 237,
710 213–221. <https://doi.org/10.1016/j.biortech.2017.04.004>

711 Spaccini, R., Cozzolino, V., Di Meo, V., Savy, D., Drosos, M., Piccolo, A., 2019.
712 Bioactivity of humic substances and water extracts from compost made by ligno-
713 cellulose wastes from biorefinery. *Sci. Total Environ.* 646, 792–800.
714 <https://doi.org/10.1016/j.scitotenv.2018.07.334>

715 Spaccini, R., Piccolo, A., 2009. Molecular characteristics of humic acids extracted from
716 compost at increasing maturity stages. *Soil Biol. Biochem.* 41, 1164–1172.
717 <https://doi.org/10.1016/j.soilbio.2009.02.026>

718 Stedmon, C.A., Bro, R., 2008. Characterizing dissolved organic matter fluorescence
719 with parallel factor analysis: a tutorial. *Limnol. Oceanogr.* 6, 1–8.
720 <https://doi.org/10.4319/lom.2008.6.572>

721 Stedmon, C.A., Markager, S., Bro, R., 2003. Tracing dissolved organic matter in aquatic
722 environments using a new approach to fluorescence spectroscopy. *Mar. Chem.* 82,
723 239–254. [https://doi.org/10.1016/S0304-4203\(03\)00072-0](https://doi.org/10.1016/S0304-4203(03)00072-0)

724 Stemann, J., Putschew, A., Ziegler, F., 2013. Hydrothermal carbonization: Process
725 water characterization and effects of water recirculation. *Bioresour. Technol.* 143,
726 139–146. <https://doi.org/10.1016/j.biortech.2013.05.098>

727 Stevenson, F.J., 1994. *Humus chemistry: Genesis, composition, and reactions*. New
728 York John Wiley Sons.

729 Swift, R.S., 1996. *Methods of soil analysis. Part 3. Chemical methods*. Soil Sci. Soc.
730 Am. 1011–1020.

731 Tadini, A. M.; Mounier, S.; Milori, D.M.B.P., 2019. Modeling the quenching of
732 fluorescence from organic matter in Amazonian soils. *Sci. Total Environ.* 698,
733 134067. <https://doi.org/10.1016/j.scitotenv.2019.134067>

734 Tadini, A.M., Constantino, I.C., Nuzzo, A., Spaccini, R., Piccolo, A., Moreira, A.B.,
735 Bisinoti, M.C., 2015. Characterization of typical aquatic humic substances in areas
736 of sugarcane cultivation in Brazil using tetramethylammonium hydroxide
737 thermochemolysis. *Sci. Total Environ.* 518–519, 201–208.

738 <https://doi.org/10.1016/j.scitotenv.2015.02.103>

739 Tang, W.W., Zeng, G.M., Gong, J.L., Liang, J., Xu, P., Zhang, C., Huang, B. Bin, 2014.

740 Impact of humic/fulvic acid on the removal of heavy metals from aqueous

741 solutions using nanomaterials: A review. *Sci. Total Environ.* 468–469, 1014–1027.

742 <https://doi.org/10.1016/j.scitotenv.2013.09.044>

743 US EPA, 2000. Environmental Protection Agency, Environmental Response Team.

744 Standard operating procedures – SOP 1–4.

745 Uyguner, C.S., Bekbolet, M., 2005. Evaluation of humic acid photocatalytic degradation

746 by UV-vis and fluorescence spectroscopy. *Catal. Today* 101, 267–274.

747 <https://doi.org/10.1016/j.cattod.2005.03.011>

748 Weiner, B., Poerschmann, J., Wedwitschka, H., Koehler, R., Kopinke, F.D., 2014.

749 Influence of Process Water Reuse on Hydrothermal Carbonization of Paper.

750 *Sustain. Chem. Eng.* 2, 2165–2171. <https://doi.org/10.1021/sc500348v>

751 Yang, F., Zhang, S., Cheng, K., Antonietti, M., 2019. A hydrothermal process to turn

752 waste biomass into artificial fulvic and humic acids for soil remediation. *Sci. Total*

753 *Environ.* 686, 1140–1151. <https://doi.org/10.1016/j.scitotenv.2019.06.045>

754 Yang, X., Tsibart, A., Nam, H., Hur, J., El-Naggar, A., Tack, F.M.G., Wang, C.H., Lee,

755 Y.H., Tsang, D.C.W., Ok, Y.S., 2019. Effect of gasification biochar application on

756 soil quality: Trace metal behavior, microbial community, and soil dissolved

757 organic matter. *J. Hazard. Mater.* 365, 684–694.

758 <https://doi.org/10.1016/j.jhazmat.2018.11.042>

759 Yuan, D.H., Guo, X.J., Wen, L., He, L.S., Wang, J.G., Li, J.Q., 2015. Detection of

760 Copper (II) and Cadmium (II) binding to dissolved organic matter from

761 macrophyte decomposition by fluorescence excitation-emission matrix spectra
762 combined with parallel factor analysis. *Environ. Pollut.* 204, 152–160.
763 <https://doi.org/10.1016/j.envpol.2015.04.030>

764 Zherebtsov, S.I., Malysenko, N. V., Bryukhovetskaya, L. V., Lyrshchikov, S.Y.,
765 Ismagilov, Z.R., 2015. Sorption of copper cations from aqueous solutions by
766 brown coals and humic acids. *Solid Fuel Chem.* 49, 294–303.
767 <https://doi.org/10.3103/S0361521915050110>

768

769

770

Table 1[Click here to download Table: Table 1.doc](#)

Table 1. Biomass, additives, temperature, and reaction time used for hydrothermal carbonization and recarbonization.

Carbonization/ Recarbonization	Reaction	Biomass	Additive (4% v/v)	Temp.	Time
HH₃PO₄	1	Vinasse Sugarcane bagasse	Phosphoric Acid	230 °C	13 h
HH₂SO₄	2	Vinasse Sugarcane bagasse	Sulfuric Acid	230 °C	13 h
RHH₃PO₄	3	Process water (from reaction1) Sugarcane bagasse	Phosphoric Acid	230 °C	13 h
RHH₂SO₄	4	Process water (from reaction 2) Sugarcane bagasse	Sulfuric Acid	230 °C	13 h

Table 2[Click here to download Table: Table 2.doc](#)

Table 2. Carbon (C), hydrogen (H), nitrogen (N), oxygen (O) and sulfur (S) contents; O/C, H/C, and C/N atomic ratios; and absorbance ratios E_{465}/E_{665} and E_{270}/E_{407} for HA and HLA samples.

HA/HLA	C (%)	H (%)	N (%)	O (%)	S (%)	O/C	H/C	C/N	E₄₆₅/E₆₆₅	E₂₇₀/E₄₀₇
TM I*	51.24	3.80	3.41	40.61	0.94	0.59	0.89	17.80	3.92	2.81
TM II*	39.62	4.05	4.04	51.37	0.92	0.97	1.23	11.38	4.33	3.43
TM III*	50.22	3.69	2.97	42.14	0.98	0.63	0.88	19.95	4.18	2.90
HH₂SO₄**	51.95	5.25	1.47	39.88	1.45	0.57	1.21	43.30	5.71	4.06
HH₃PO₄**	62.27	5.62	2.60	28.47	1.04	0.34	1.08	28.83	5.33	3.93
RHH₂SO₄**	48.90	4.46	1.20	37.99	7.45	0.58	1.09	51.00	3.50	3.33
RHH₃PO₄**	53.54	4.82	1.83	35.92	0.89	0.50	1.08	34.31	4.67	3.19

* natural humic acids; ** humic-like acids

Table 3. Relative value (% of total area) and indexes obtained from ¹³C-CPMAS- NMR spectra of HA and HLA samples.

HA/HLA	¹³ C NMR region (ppm)							¹³ C NMR indexes		
	220-190	190-160	160-145	145-110	110-60	60-45	45-0	ARM	A/OA	HB/HI
TM I*	4.93	15.41	5.86	34.98	17.87	5.55	15.41	1.23	0.86	1.45
TM II[#]	-	-	-	-	-	-	-	-	-	-
TM III*	6.43	14.11	4.98	30.08	17.22	6.43	20.75	0.92	1.20	1.48
HH₂SO₄**	1.75	6.11	6.55	33.62	3.06	5.24	43.67	0.86	14.29	5.19
HH₃PO₄**	2.55	2.55	3.57	29.59	1.02	9.69	51.02	0.64	50.00	5.32
RHH₂SO₄**	3.03	5.30	7.95	42.80	2.65	0.38	37.88	1.25	14.29	7.80
RHH₃PO₄**	1.79	1.79	8.04	36.16	0.45	7.14	44.64	0.98	100.00	7.96

* natural humic acids; ** humic-like acids; [#] not realized / ARM = aromaticity index $[(110 - 160) / \Sigma (0 - 45) + (60 - 110)]$; A/OA = alkyl/O-alkyl index $(0 - 45) / (60 - 110)$; HB/HI = hydrophobicity index = $[\Sigma (0 - 45) + (110-160) / \Sigma (45 - 60) + (60 - 110) + (160 - 190)]$.

Table 4. Log K, CL, CC, and bias values for components 1 and 2 regarding the interaction of HA and HLA with Cu(II) ions.

HA/HLA	Component 1				Component 2			
	Bias	CL (mol L ⁻¹)	Log K	CC (mmol of Cu g ⁻¹ C)	Bias	CL (mol L ⁻¹)	Log K	CC (mmol of Cu g ⁻¹ C)
TM I*	2.25	6.50E-06	5.36	1.27	4.18	3.50E-06	5.58	0.68
TM II*	0.96	6.70E-06	5.41	1.69	2.18	3.20E-06	5.60	0.81
TM III*	1.98	8.00E-06	5.30	1.59	2.29	4.50E-06	5.59	0.90
HH ₂ SO ₄ **	2.04	2.40E-05	4.89	4.62	2.67	1.00E-05	5.09	1.92
HH ₃ PO ₄ **	0.47	2.40E-05	4.88	3.85	0.49	1.70E-05	5.06	2.73
RHH ₂ SO ₄ **	0.71	3.20E-05	4.89	6.54	0.77	2.50E-05	5.08	5.11
RHH ₃ PO ₄ **	0.27	1.80E-05	4.90	3.36	0.35	1.40E-05	5.09	2.61

* natural humic acids; ** humic-like acids

Figure 1

[Click here to download Figure: Figure 1.doc](#)

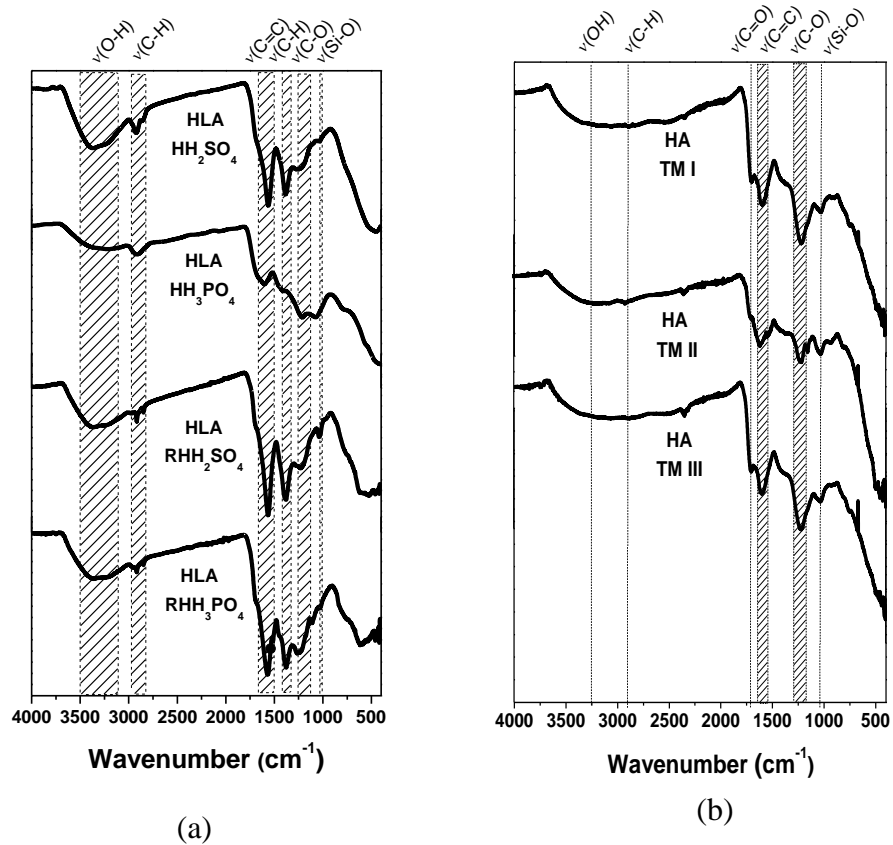


Fig.1. FTIR spectra for HLA isolated from hydrochar (a) and HA isolated from soil (b).

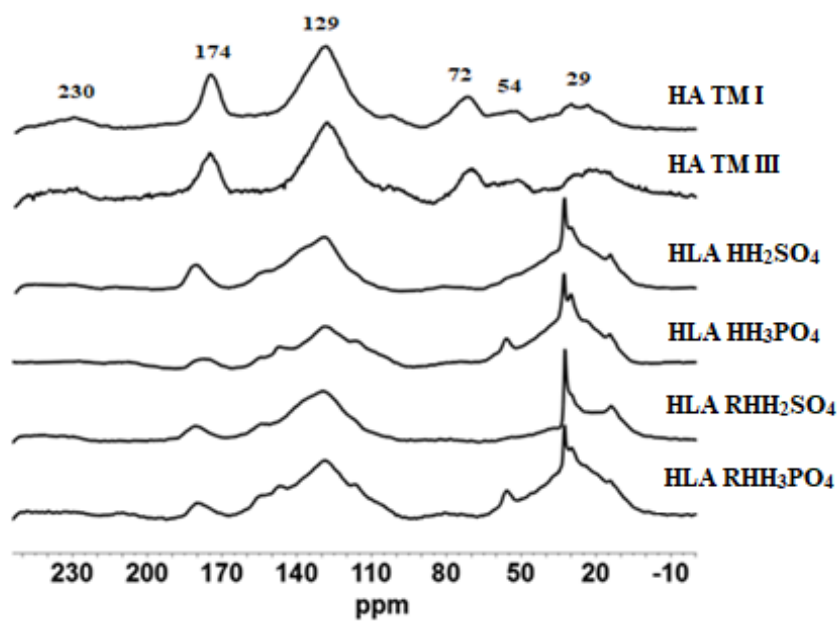


Fig.2. Solid-state ^{13}C NMR spectra of HA and HLA.

Figure 3

[Click here to download Figure: Figure 3.doc](#)

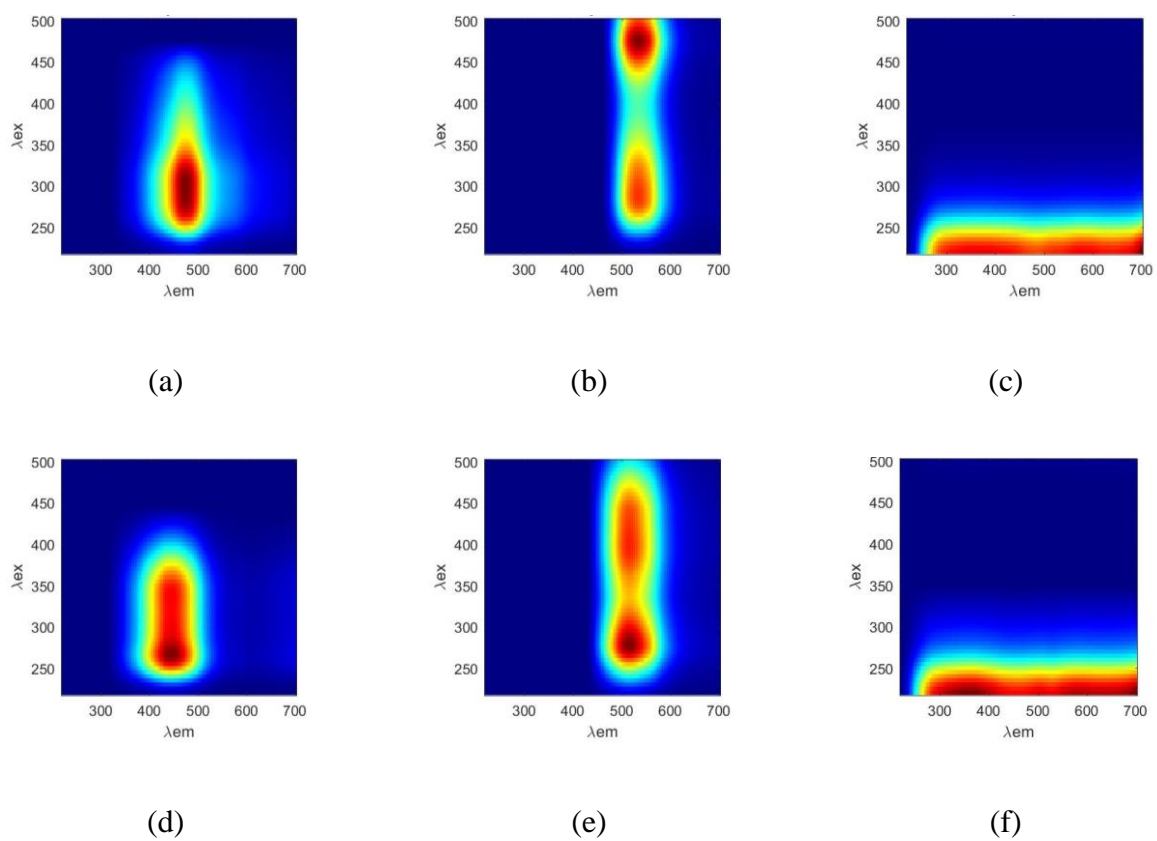


Fig. 3. Components 1, 2, and 3 obtained by CP/PARAFAC for interaction of HA (a, b and c, respectively) and components 1, 2, and 3 for interaction of HLA (d, e and f, respectively) with Cu(II) ions.

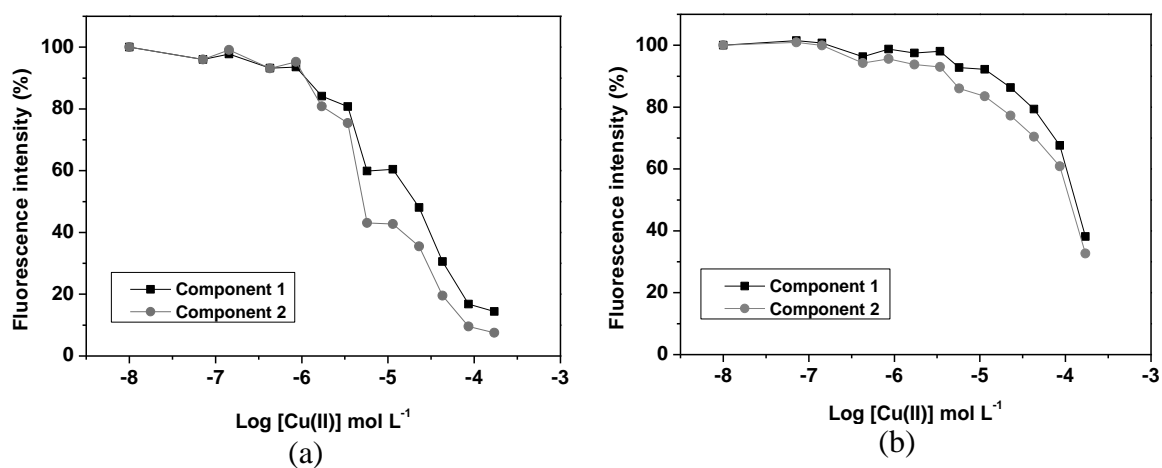
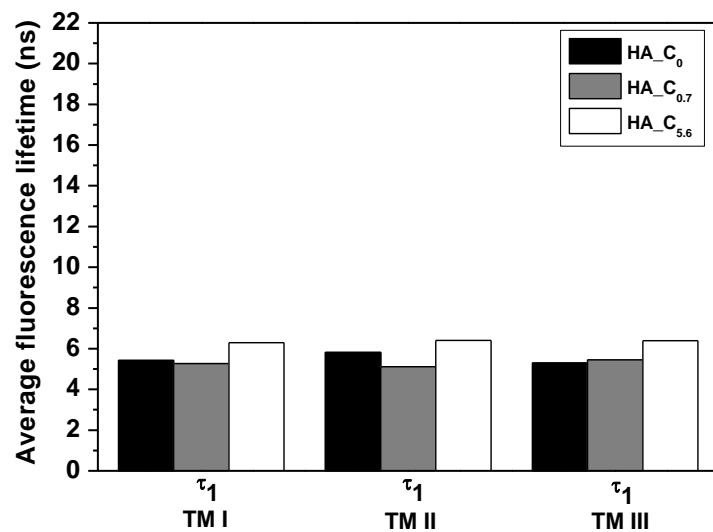


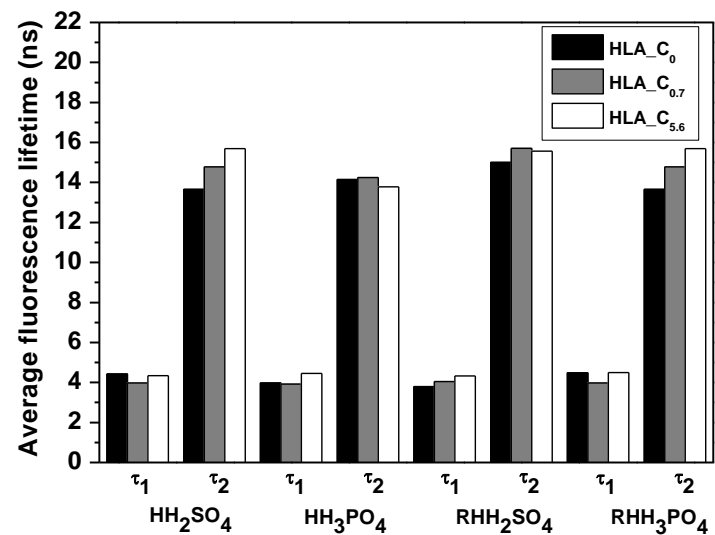
Fig. 4. Contribution of relative fluorescence intensity for components 1 and 2 regarding the interaction of TM I HA (a) and HH₂SO₄ HLA (b) with Cu (II) ions.

Figure 5

[Click here to download Figure: Figure 5.doc](#)



(a)



(b)

Fig. 5. Average fluorescence lifetime distribution for HA (τ_1) (a) and HLA (τ_1 and τ_2) (b) when interacting with Cu(II) ions at concentration:

C_0 = no copper added, $C_{0.7}$ = 0.7 mg L^{-1} and $C_{5.6}$ = 5.6 mg L^{-1} .